PCCP

Accepted Manuscript

ROYAL SOCIETY OF CHEMISTRY

www.rsc.org/pccp

A new understanding of bond torsion reveals a bond-path doesn't rotate in concert with the nuclei of the rotated group.

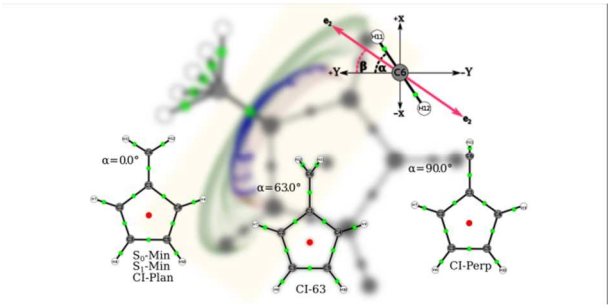

THE RESPONSE OF THE ELECTRONIC STRUCTURE TO ELECTRONIC EXCITATION AND DOUBLE BOND TORSION IN FULVENE: A COMBINED QTAIM, STRESS TENSOR AND MO PERSPECTIVE

Samantha Jenkins[a]*, Lluìs Blancafort[b]*, Steven R. Kirk[a], Michael J. Bearpark[c]

[a]*Key Laboratory of Chemical Biology and Traditional Chinese Medicine Research (Ministry of Education of China) and Key Laboratory of Resource Fine-Processing and Advanced Materials of Hunan Province, College of Chemistry and Chemical Engineering,*

[a]*Hunan Normal University, Changsha Hunan 410081, China.*

[b]*Institut de Quimica Computational and Departament de Quimica,Universitat de Girona, Spain.*

[c]*Department of Chemistry, Imperial College, London, SW7 2AZ, UK*

New insights into the double bond isomerization of fulvene in the ground and excited electronic states are provided by newly developed QTAIM and stress tensor tools. The S_0 and S_1 states follow the 'biradical' torsion model, but the double bond is stiffer in the S_0 state; by contrast, the S_2 state follows the 'zwitterionic' torsion. Differences are explained in terms of the ellipticity and bond critical point (BCP) stiffness for both QTAIM and the stress tensor. Overall, the wave-function based analysis is found to be in agreement with the work of Bonacic-Koutecky and Michl that the bond-twisted species can have biradical or zwitterionic character, depending on the state. Using QTAIM and the stress tensor a new understanding of bond torsion is revealed; the electronic charge density around the twisted bond is found not to rotate in concert with the nuclei of the rotated $–CH_2$ methylene group. The ability to visualize how the bond stiffness varies between individual electronic states and how this correlates with the QTAIM and stress tensor bond stiffness is highlighted. In addition, the most and least preferred morphologies of bond-path torsion are visualized. Briefly we discuss the prospects for using this new QTAIM and stress tensor analysis for excited state chemistry.

I. Introduction

Double bond torsion in organic molecules is fundamental [1] in chemistry. In molecules that have this functionality, the orientation of the double bond substituents gives rise to isomers with different properties. In the ground state, the barrier for rotation of non-conjugated bonds is estimated to be of the order of 60 kcal/mol [2]. Therefore, double bond isomers can be considered thermally stable with regard to isomerization. By contrast, double bond isomerization in excited states is often an energetically favored process[1]. The most prominent example is the retinal chromophore, a molecule for which the isomerization of a double bond, triggered by visible light, occurs in less than 1 ps [3]. This process is at the basis of vision. Here we study the double bond isomerization in the ground and excited states of fulvene, see Figure 1, a benchmark molecule for excited states methods that has been studied extensively [4–11]. Using the structures optimized in previous studies we focus on the electronic structure changes that occur during the evolution of the molecule on the S_1 excited state surface and its decay to the ground state at a conical intersection seam. While excited state processes are usually analyzed in the frame of MO theory, here we apply the quantum theory of atom in molecules (QTAIM) [12–15] in combination with the electronic stress tensor [16–22], see section 2.1 for more explanation on the definitions of QTAIM and the stress tensor.

In particular, we want to apply for the first time both the QTAIM and stress tensor responses β, see Figure 1 and the stress tensor ellipticity and bond stiffness to understand bond torsion. Up to now, QTAIM-based descriptors have been mostly applied to study electronic structure and reactivity in the electronic ground state and here we investigate their applicability to the excited state. Therefore, we want to investigate to what extent QTAIM and the stress tensor can be applied to excited states and whether they are able to track the changes induced by electronic excitation and also the changes in electronic structure along the reaction coordinate. To assess this, we complement our QTAIM analysis with a wave function based method, namely the spin density matrix elements (P_{ij}) of a CASSCF function with localized orbital basis [23].

As we explain below, our description of double bond torsion is in line with the well-known picture established by Bonacic-Koutecky and Michl [24] where this process can take place through biradical or

zwitterionic structures. However, the QTAIM and stress tensor analysis provides new insight into the response of the charge density to the double bond torsion that goes beyond this picture. Thus, we follow the response of the electronic charge density to nuclear rotation in a quantitative, quantum mechanically consistent way. From now on for clarity we will refer to the 'electronic charge density' as the 'charge density'. Contrary to what one may assume, the charge density does not always rotate in accordance with the nuclei. Instead the resistance of the charge density to rotation depends on the electronic state, and the behavior of the charge density also differs locally, depending on which direction of the bond path frame we consider.

The preferred direction of charge density accumulation is associated with the QTAIM $\mathbf{e}_2$ eigenvectors, and the inverse is true for the $\mathbf{e}_1$ eigenvectors. In turn, the stress tensor $\mathbf{e_1}$ eigenvector gives the direction along which it is most difficult to distort the charge density. We associate the QTAIM $\mathbf{e}_2$ and stress tensor $\mathbf{e_1}$ eigenvector directions with the π density corresponding to the double bond. Thus, by following the rotation of both vectors around the C_1-C_6 bond critical point (BCP) we get a picture of how the C_1-C_6 bond-path *framework* twists during the rotation of the double bond. We define the bond-path framework in the sub-section '*QTAIM -Bond-path torsion'* of section 2.1.

In section 2 of this work we outline the QTAIM and stress tensor theory terminology and new concepts, including bond-path stiffness, used (section 2.1), valence bond analysis (section 2.2), and computational details (section 2.3). In section 3 we present our results and our conclusions in section 4.

2. Theory and methods

2.1 QTAIM theory and the stress tensor

QTAIM, BCP descriptors; the ellipticity ε, the $\underline{\mathbf{e_1}}$ *and* $\underline{\mathbf{e_2}}$ *eigenvectors and stiffness* S

In this work we use descriptors derived from the charge density distribution $\rho(\mathbf{r})$ in the framework of the QTAIM. In particular, we use the eigenvalues and eigenvectors of the Hessian matrix of the charge density, $\nabla\nabla^T\rho(\mathbf{r})$, at the bond critical points. The eigenvalues are labeled in increasing order, $\lambda_1 < \lambda_2 < \lambda_3$, with λ_1, $\lambda_2 < 0$. The pair of special gradient paths linking a BCP with two nuclei and along which ρ is a maximum with respect to any neighboring path is known as an atomic interaction line (AIL). In the limit that the forces on

the nuclei become vanishingly small an AIL becomes a bond-path, although not necessarily a chemical bond [25]. The complete set of critical points and bond-paths of a molecule or cluster is referred to as the molecular graph.

Closed shell interactions, e.g., ionic bonds and hydrogen bonds are characterized by positive values of the Laplacian $\nabla^2\rho(\mathbf{r}_b)$, low $\rho(\mathbf{r}_b)$ values < 0.1 atomic units and values of $|\lambda_1|/\lambda_3 < 1$; these types of interactions are dominated by the contraction of charge away from the BCP toward each of the nuclei. Conversely, shared interactions, e.g., covalent or sigma bonds, have both negative $\nabla^2\rho(\mathbf{r}_b)$ values and high values of $\rho(\mathbf{r}_b)$ as well as values of $|\lambda_1|/\lambda_3 > 1$. The ratio $|\lambda_1|/\lambda_3$ also previously defined the bond-path 'softness' [12] where larger values indicate a higher degree of softness.

We can also define an ellipticity $\varepsilon = (\lambda_1/\lambda_2) - 1$, as a measure of the relative accumulation of charge in the two directions $\underline{\mathbf{e}}_1$ and $\underline{\mathbf{e}}_2$ perpendicular to the bond-path at a BCP. The third eigenvector $\underline{\mathbf{e}}_3$ is associated with the λ_3 eigenvalue and indicates the direction of the bond-path at the BCP. The most and least preferred directions of electron accumulation are $\underline{\mathbf{e}}_2$ and $\underline{\mathbf{e}}_1$, respectively [26–28]. The QTAIM ellipticity ε provides a measure of π and σ bond character; larger values (> 0.1) indicate π bond character and lower ε values indicate σ bond character. The ellipticity ε also defines the topological instability of a BCP, the higher the ε value the more unstable the bond [27], independent of the strength of the bond or even the curvature of the bond-path.

For this work we introduce a bond-path stiffness $S = \lambda_3/|\lambda_2|$ based on the physical intuition that the form of the QTAIM stiffness will be the reciprocal of the QTAIM softness $|\lambda_1|/\lambda_3$. For the QTAIM stiffness S to be physically meaningful it should contain the λ_2 eigenvalue to be consistent with the $\underline{\mathbf{e}}_2$ eigenvector which indicates the direction of preferred accumulation of charge density and hence the direction of the π bond.

QTAIM -Bond-path torsion

To describe the torsion of a bond-path within QTAIM we define the bond-path *framework* as the set of orthogonal $\underline{\mathbf{e}}_1$, $\underline{\mathbf{e}}_2$ and $\underline{\mathbf{e}}_3$ eigenvectors *and* the basin path sets of the two bonded nuclei that comprise the torsional bond-path, see Figure 5 and the accompanying figure caption. We define the basin path set using a plane defined using either a single plane normal vector, or a pair of non-collinear vectors in the plane

passing through a specified point in space. The basin path set is a set of trajectories of a vector function e.g. the gradient of the charge density, seeded at equidistant points around the circumference of a circle of small radius centred on the specified point and lying in the specified plane. The trajectories terminate where the charge density falls below 0.001 a.u; they are not restricted to lie in the original seeding plane but rather go where the local direction of the vector function dictates.

With the QTAIM definition of the bond-path framework in place there is no difficulty in describing a bond-path framework as being twisted. We will use the term 'bond-path torsion' or similar to mean bond-path *framework* torsion from now on in this investigation.

For the BCP of a twisted bond-path with non-negligible ellipticity ε we can always define a non-zero bond-path torsion. The orientation of the eigenvector $\underline{\mathbf{e}}_3$ associated with the bond-path direction does not change during the rotation, but information about the response of the bond-path to the twist can be found from the $\underline{\mathbf{e}}_1$ and $\underline{\mathbf{e}}_2$ eigenvectors that are always perpendicular to the $\underline{\mathbf{e}}_3$ eigenvector. The reason is that the relative orientation of the $\underline{\mathbf{e}}_1$ and $\underline{\mathbf{e}}_2$ eigenvector framework will rotate about the fixed $\underline{\mathbf{e}}_3$ eigenvector with an applied rotation and hence the orientations of the $\underline{\mathbf{e}}_1$ and $\underline{\mathbf{e}}_2$ eigenvector vary uniquely, whilst still always being orthogonal to each other and to the $\underline{\mathbf{e}}_3$ eigenvector, see Figure 1.

Firstly, we explore the torsion of the C_1-C_6 BCP bond-path in the frame of reference of the five carbon ring for the C_1 nucleus and in the frame of the methylene group for the C_6 nucleus as the methylene group is rotated, see Figure 1 and Figure 5(a-c). Secondly, the frame of reference of the $\underline{\mathbf{e}}_1$ and $\underline{\mathbf{e}}_2$ eigenvectors at the C_1-C_6 BCP bond-path torsion was considered. This was done by choosing the trajectory plane for basin path set calculation defined by the plane containing the C_1-C_6 BCP bond-path and either the $\underline{\mathbf{e}}_2$, see Figure 5(d) or the $\underline{\mathbf{e}}_1$ eigenvector, refer to Figure 5(e).

The quantum stress tensor $\boldsymbol{\sigma}(\mathbf{r})$

The quantum stress tensor $\boldsymbol{\sigma}(\mathbf{r})$ [16–22], which is directly related to the Ehrenfest force $\mathbf{F}(\mathbf{r}) = -\nabla\cdot\boldsymbol{\sigma}(\mathbf{r})$, at the BCPs of the charge density provides insight into the low frequency 'normal electronic modes' that accompany structural dynamics and rearrangements [29]. The stress tensor $\underline{\mathbf{e}}_2^{\boldsymbol{\sigma}}$ eigenvectors should reflect the imposed external torsion on the electronic bond.

The quantum stress tensor, $\boldsymbol{\sigma}(\mathbf{r})$ has been found to be a vital quantity whereby the 'mechanics' of an atom in a molecule can be determined [32]. Within the stress-tensor electron-preceding perspective [30] the point along the bond-path where the forces on the electrons vanish is sometimes referred to as the Lorentz point [17,33]. Recently [27], it was found that the stress tensor the ratio $|\lambda_1|/\lambda_3$ cannot be used distinguish between shared shell and closed shell interactions in contrast with QTAIM as previously mentioned. In this work we use the same ratio as the stress tensor stiffness S_σ, applied to double bond torsion. The rationale behind our choice for S_σ is that the $\mathbf{e_1}^{\boldsymbol{\sigma}}$ eigenvector indicates the direction of the π bond, so that larger values of $|\lambda_1|$ correspond to stronger, stiffer π bonds.

In this work we are calculating the stress tensor properties using the QTAIM partitioning scheme and not a stress tensor partitioning scheme, we will use the Bader definition of the stress tensor [4,5]. The consequence of this is that the positions of BCPs along a given bond-path in the two partitioning schemes can be rather different, particularly for bond-paths where the BCP is closer to one nucleus than the other, e.g for the C-H sigma bond BCP bond-paths. Therefore, to ensure that we have a close representation of the stress tensor properties at a BCP using the QTAIM partitioning scheme we only use the stress tensor properties from BCPs positioned very close to the geometric mid-point of a bond-path. Therefore, for this work only the stress tensor properties of the C-C BCPs and not the C-H BCPs will be examined because C-H BCPs are not at the geometric mid-point of the bond-path. It is highly likely that the position of the C-H BCPs for the QTAIM and stress tensor partitioning would be in different positions along the C-H BCP and so the calculated values of the stress tensor at the QTAIM BCP would be different from those calculated at the actual stress tensor BCP.

2.2 Valence-bond based bonding analysis

To complete the QTAIM-based analysis we use a valence-bond (VB) based method for the analysis of bonding in organic molecules [23]. The method is based on the coefficients of the spin exchange density matrix **P** of a complete active space self-consistent field (CASSCF) wave function, calculated with a

localized orbital basis. With this basis, the CASSCF determinants become VB like determinants with different spin coupling patterns. The P_{ij} indices evaluate the contributions of the determinants to the CASSCF wave function and can be used to generate resonance formulas. In practice, we use the $\alpha\beta$ components of the spin exchange density matrix, which have the following formula (Eq. 1):

$$P_{ij}^{\alpha\beta} = \frac{1}{2}\sum_{K,L} c_K c_L \left\langle \phi_K \left| a_{i\alpha}^{+} a_{j\alpha} a_{j\beta}^{+} a_{i\beta} \right| \phi_L \right\rangle \qquad (1)$$

When the active space consists of the whole π system of the molecule, an index $P_{ij} > 0.3$ between two neighboring centers can be interpreted as a π bond. P_{ij} values of zero correspond to uncoupled electron pairs, while negative P_{ij} indices can be understood as triplet coupled electron pairs. Together with the P_{ij} indices, we have used the occupations of the localized active space orbitals (diagonal elements of the one electron density matrix). The changes in the occupations are an indication of charge transfer during the excitation.

2.3 Computational Details

The structures considered in this work, including the conical intersections, have been optimized in our previous studies on the photophysics of fulvene [4,10,34]. The wave function has been calculated at the CASSCF/cc-pvdz level of theory with an active space of six electron in six orbitals, i.e. (6,6), averaging over three states. The calculations have been carried out with Gaussian 03(E1)[35]. The subsequent QTAIM and stress tensor analysis was performed using the AIMStudio package [36]. At the conical intersections where the S_0 and S_1 states are degenerate, we use the charge density of the symmetry adapted states for consistency with the remaining structures. The sets of atomic basin paths for the C_1 and C_6 nuclei were all 'seeded', with starting points equally distributed around a small (0.05 Ångstrom) circle around each nucleus, in the plane defined by the C_6, C_2 and C_4 nuclei with 112 paths per nuclei, see Figure 1 and the accompanying figure caption.

3. Results and discussion

The double bond isomerization in the different electronic states of fulvene is studied here in the context of its photophysics. In Figure 1(a) we show the definition of the torsion angle α, and in Figure 1(b-d) we show the relevant structures for our study. Fulvene is not fluorescent because there is a very favorable radiationless decay from the first excited to the ground state at a conical intersection [30]. The excited state decay paths along the relevant coordinates Q_1 (symmetric bond alternation) and Q_2 (methylene torsion) are shown schematically in Figure 2. After excitation to S_1, the decay coordinate Q_1 goes along planar structures of C_{2v} symmetry where the angle α is zero, see Figure 1 and Figure 2(a). Thus, it goes from **S_0-Min** to the minimum of the S_1 excited state, **S_1-Min**, and further to a planar conical intersection, **CI-Plan**. **CI-Plan** is part of an extended seam of intersection along the methylene bond torsion coordinate Q_2, see Figure 2(b). The global energy minimum of the seam is a of C_2 symmetric structure where the methylene group is twisted away from the ring (α = 63.0°), **CI-63**, and there is also a structure with a perpendicular methylene group (α = 90.0°), **CI-Perp**, of C_{2v} symmetry. We consider the three structures on the seam because dynamics calculations show that the decay can take place all along the extended seam, and not just at its minimum energy point [4,6,8]. The results are summarized in Tables 1–6 and Figures 4 and 5, where the states are labeled by symmetry.

3.1 Bonding picture of the three states at S_0-Min

The ability to differentiate between different electronic states is a necessary first step when considering the application of QTAIM to analyzing excited states and their associated phenomena. Therefore we start analyzing the changes in electronic structure for the different states at **S_0-Min** (ground state minimum structure). In a previous work on the excited state aromaticity of some fulvene derivatives, the S_1 state is characterized by large changes in the dipole moment along the z-axis, of 5 - 10 D [38]. However, in the unsubstituted case the changes in the dipole moment upon excitation from S_0 to S_1 and S_2 are smaller than 1 D, and the main change in the wave function lies in the bonding pattern. Therefore, we examine the variation of the QTAIM ellipticity ε at the CC bond critical points (BCP), see section 2 for a definition of ε, and we compare with the P_{ij} analysis. Comparing the data in Tables 1 for the ellipticity (ε) and Table 2 for

(P_{ij}) it can be seen that BCPs with values of QTAIM ellipticity $\varepsilon \geq 0.3$ are describable as double bonds or π bonds e.g. S_0 state, C_1-C_6, while BCPs with $\varepsilon < 0.1$ are associated with single bonds or σ bonds. We can see that using QTAIM we can describe a continuum of bonding character with the QTAIM ellipticity ε ranging from 0.006 to 0.365, see Table 1. For an example of the effect of the electronic excitation we see that at **S_0-MIN**, the ellipticities of the C_1-C_6 BCP at the ground and first excited states are 0.344 and 0.130 respectively indicating double and single bond character respectively, see Table 1. The P_{ij} values for the C_1-C_6 bond are 0.592 and -0.048 respectively, see Table 2, indicating the same double and single bond characterization as the QTAIM descriptor, the ellipticity. In another example, the C_3-C_5 BCP/bond we see that the excitation again changes the bonding character, but this time from single to double bond, again the QTAIM and P_{ij} indicators are in agreement.

The *Pij* and QTAIM analyses are also useful to derive resonance structures for the three states. For the ground state, the P_{ij} and QTAIM analyses describe well localized π bonds between the (C_1-C_6) and the equivalent (C_2-C_3) and (C_4-C_5) carbon atom pairs, see Figure 1 for the atom labeling scheme. Thus, the ellipticities for these bonds are 0.344 and 0.365, respectively, and the P_{ij} elements for the three bonds are 0.592. The ellipticities and P_{ij} elements of the remaining bonds are substantially lower, approximately 0.10 and 0.07, respectively. This description agrees with the conventional resonance structure of S_0; see Figure 3(a). The bond pattern is reverted in S_1. Here the highest ellipticities are found for the C_3-C_5 bond and the equivalent C_1-C_2 and C_1-C_4 bonds, 0.301 and 0.269, respectively, which have also the largest P_{ij} elements, 0.453 and 0.291, respectively. This situation, where there are stronger bonds between the C_1-C_2, C_1-C_4 and C_3-C_5 atom pairs, can we described with the resonance structure shown in Figure 3(b). Finally, in S_2 we find double bond character along the C_1-C_6 and C_3-C_5 bonds, with ellipticity values 0.274 and 0.245, P_{ij} elements 0.406 and 0.274, respectively, with lower indices in the remaining bonds. This gives the resonance structure shown in Figure 3(c). To summarize, the results for **S_0-Min** show that the QTAIM ellipticities are capable of differentiating between the bonding patterns of the ground and excited states and the results are in line with the MO-based P_{ij} analysis.

3.2 Bonding changes along the planar relaxation coordinate

Now we turn to the changes along the planar excited state relaxation coordinate. This coordinate is formed by the three structures **S_0-Min**, **S_1-Min** and **CI-Plan**, obtained in previous work. In Table 3 we present the bond-path lengths (BPL) in Ångstrom from the QTAIM analysis. The BPL coincide with the interatomic distances (bond lengths), since all bond-paths correspond almost exactly to a straight line between the atom nuclei. Along the S_1 relaxation coordinate, the C_1-C_6 and C_2-C_3/C_4-C_5 bond-paths get longer, and the C_1-C_2/C_1-C_4 and C_3-C_5 ones get shorter. For instance, the C_1-C_6 distance increases from 1.349 Å at **S_0-Min** to 1.498 Å at **S_0-Min** and 1.578 Å at **CI-Plan**. At the same time, the C_3-C_5 distance decreases from 1.484 Å at **S_0-Min** to 1.361 Å at **S_1-Min** and 1.320 Å at **CI-Plan** These changes follow the bond character described in the previous section for S_1 at the **S_0-Min** structure, i.e. a reversal of the bond pattern with respect to the ground state, where the C_3-C_5 bond has higher ellipticity (0.301) than the C_1-C_6 one (0.130). The QTAIM ellipticity can also track the changes in the bonding pattern with geometry, along any particular state, see Table 1. Thus, as the C_1-C_6 bond is stretched, the ellipticities for the three states decrease. For instance, the ellipticity of S_0 decreases from 0.344 (**S_0-Min**) to 0.252 (**S_1-Min**) and 0.229 (**CI-Plan**). Inversely, as the C_3-C_5 is compressed, the ellipticities increase. For instance, the S_0 ellipticities are 0.102 (**S_0-Min**) to 0.158 (**S_1-Min**) and 0.183 (**CI-Plan**).

Turning to the proposed QTAIM descriptor for the double bond stiffness, $S = \lambda_3/|\lambda_2|$, from our previous analysis it can be expected that the double bond stiffness should decrease upon excitation, particularly for the S_1 state, since the ellipticities and P_{ij} values decrease. The stiffness should also decrease as the C_1-C_6 bond is stretched, going from **S_0-Min** to **S_1-Min** and **CI-Plan**. The values of S in Table 4 show that, indeed, the stiffness decreases upon excitation, but as the C_1-C_6 is stretched the values of S increase. For instance, the S_0 stiffness increases from 0.601 at **S_0-Min** to 0.774 at **S_1-Min** and 0.821 at **CI-Plan**. This is against chemical intuition, since the bond should become less stiff when stretched, *i.e.* weaker and less resistant to the twist, and it suggests that the proposed expression is not a good descriptor for the double bond stiffness.

To summarize the results of the last two sections, the QTAIM ellipticity is able to follow the changes in the bonding pattern induced by the excitation and changes in the geometry. From the good agreement with the

well-known MO picture, we can conclude that QTAIM ellipticity provides the correct picture for the charge density of the excited states. In contrast to this, the proposed QTAIM stiffness descriptor

$S = \lambda_3/|\lambda_2|$ does not behave as expected, since it predicts an increase of the stiffness as the C_1-C_6 bond is stretched.

3.3 Relationship between QTAIM and stress tensor ellipticities

In the preceding sections we have shown that the ellipticity of the charge density ε is able to describe the changes that occur during the excited state relaxation. Now we turn our attention to the ellipticity of the stress tensor ε_σ. We will show that the two parameters ε and ε_σ are correlated.

We can compare the variation of the QTAIM ellipticity ε with the stress tensor ellipticity ε_σ to explore any relation between the two quantities, see Table 1 for the states of the **CI-63** structure, section 2 for a definition of ε_σ and also see Figure 4 and the corresponding figure caption. The relationship between ellipticities of the torsional C_1-C_6 BCPs is denoted in each case by a dashed line and that of the remaining C-C BCPs by a solid line, see Figure 4. From the figure captions it can be seen that the relationship in all cases between the stress tensor ellipticity ε_σ and the QTAIM ellipticity ε is rather linear. For each of the non-torsional BCPs the gradient is 0.5, however, the gradients for the C_1-C_6 torsional bonds increase as the angle α increases from α = 0.0°- 90.0°, they vary between 0.46 and 0.67 for α = 0.0° and 90.0° respectively, see Figure 4.

The ellipticity values ε and ε_σ plotted in Figure 4 show that there are two types of BCP. The first group is the BCPs which form part of the conjugated π system, where the correlation between the QTAIM and stress tensor ellipticities, ε and ε_σ, have similar gradients and intercepts. For all states, at planar geometries, the plots of the C_1-C_6 BCP ellipticities have similar gradient to those for the remaining C-C BCPs, which means that the C_1-C_6 π bond-path is conjugated with the five member ring, see Figure 4(a). By contrast, at non-

planar geometries the plots of the C_1-C_6 BCP ellipticities have a different gradient to those for the remaining C-C BCPs and the difference gets larger as the value of the α angle increases; see Figure 4(b) and Figure 4(c) for values of the α angle of 63° and 90° respectively. This is an indication of the fact that the methylene group becomes increasingly deconjugated from the five-membered ring as it is rotated ~~and the C_1-C_6 loses its π bond character~~. Further we predict that all other values of α will yield a series of linear relations between stress tensor ellipticity ε_σ and the QTAIM ellipticity ε where the intercepts with the X-axis of the plots of the C_1-C_6 BCP data lie between 0.06 and 0.00 corresponding to α = 0.0° and 90.0° respectively. The twisting of the C_1-C_6 bond-path results in higher relative values of the stress tensor ellipticity ε_σ of the BCPs of the five-membered ring as compared with the QTAIM ellipticity ε as seen from the increased values of the gradient for the plots of the C_1-C_6 BCP data in Figure 4(a-c), see also Table 1 and the accompanying footnote.

To summarize, a good correlation holds between the QTAIM and stress tensor ellipticities ε and ε_σ, respectively, for all conjugated bonds in the plane of the ring, regardless of the order of the bonds. However, as the CH_2 group is twisted, this group becomes progressively decoupled from the ring, resulting in increases of the gradient of the plot of C_1-C_6 BCP ellipticity data.

3.4 Bonding changes along the torsion coordinate

Ellipticities, P_{ij} elements and resonance structures

Let us now focus on the changes of electronic structure along the torsion coordinate. We start with the ellipticities and the P_{ij} elements at the perpendicular **CI-Perp** structure, see Tables 1 and 2 respectively. The proposed resonance structures for the states are shown in Figure 3(d-g). At **CI-Perp**, the S_0 and S_1 states are energetically degenerate. The methylene twist generates a biradical structure, with a delocalized radical on the five member ring and a localized radical on the C_6 carbon. The state degeneracy can be understood in terms of the two degenerate states of the cyclopentadienyl radical, which have quinoid-like and anti-quinoid like resonance structures, see Figure 3(d) and 3(e) [31].

The QTAIM and VB-based analyses, see Tables 1 and 2 agree with this picture. In S_0, with A_2 symmetry at **CI-Perp**, the ring has quinoid-like electronic structure, with double bonds between the C_2-C_3 and C_4-C_5 pairs with ellipticity, $\varepsilon = 0.293$, P_{ij} element = 0.487 and the electron localized on C_1. In turn, the B_1 state has anti-quinoid-like character, with a double bond between C_3-C_5 nuclei where the ellipticity, $\varepsilon = 0.319$, P_{ij} element = 0.541 and three electrons delocalized over the C_2-C_1-C_4 centers with ellipticity values for C_1-C_2 and C_1-C_4 BCP/bonds, $\varepsilon = 0.254$, P_{ij} elements = 0.367. For both states the biradical character is also indicated by the small ellipticity values at the C_1-C_6 BCP; $\varepsilon = 0.025$ and 0.012 for S_0 and S_1, respectively. In this context, it is interesting to note that the VB-based analysis gives a large P_{ij} element for the C_1-C_6 bond on the S_0 state, of 0.556. This value indicates that, in the VB picture, the electrons on C_1 and C_6 are formally singlet coupled because they have opposite spins, but the QTAIM analysis shows that, exceptionally, the VB coupling cannot be interpreted as a double bond between the two carbon nuclei.

In contrast to the two lowest states, S_2, of A_1 symmetry, has a zwitterionic character at **CI-Perp**, where the two electrons of the C_1-C_6 double bond shift to the ring, leaving a negatively charged ring and a positive charge on C_6. This picture is confirmed by the occupations of the localized orbitals of the CASSCF wave function, see Table 2, where the p orbital on C_6 has occupation 0.000 and the sum of the orbital occupations on the remaining carbon atoms is 6.000. Similarly, the calculated Bader charge on C_6 is 0.812, see Table 5. The charge transfer in S_2 is favored by the formation of a six-electron, aromatic system on the ring, as evidenced by the ellipticities for the CC bonds on the ring for this state, which have values between 0.264 and 0.338. Similarly, the P_{ij} elements for these bonds lie between 0.212 and 0.333. The charge shift for S_2 is only seen at **CI-Perp**, but not for the planar and partially twisted structures. This shows that the charge shift only occurs when the CH_2 group is fully twisted.

In the following subsections we examine the response of the electronic structure to the twist using the magnitudes associated to the $\underline{\mathbf{e}}_1$-$\underline{\mathbf{e}}_2$-$\underline{\mathbf{e}}_3$ framework in the QTAIM and stress tensor pictures. Normally structural deformations result in the movement of BCPs and their associated bond-paths. However, in this case the C_1-C_6 BCP remains fixed. Moreover, all our structures have a C_2 rotation axis through the C_1-C_6 bond. By symmetry, the C_1-C_6 bond-path is linear and there is absolutely no bond-path curvature, for all

molecular graphs. For this reason, the $\underline{\mathbf{e}}_3$ eigenvector, which lies along the C_1-C_6 axis, also remains fixed, while the $\underline{\mathbf{e}}_1$ and $\underline{\mathbf{e}}_2$ eigenvectors rotate around this axis. In our QTAIM analysis we center on the $\underline{\mathbf{e}}_2$ eigenvector, which usually lies in the direction of the π electron density simply because this is where the electron density is accumulating most readily. In turn, in our stress tensor analysis we focus on the least facile eigenvector of the stress tensor ($\underline{\mathbf{e}}_1^{\sigma}$). This vector gives the direction along which the energy penalty to deform the electronic cloud, pushing the density away from the BCP, is highest. This direction corresponds to that of the π electron density. The directions of $\underline{\mathbf{e}}_2$ and $\underline{\mathbf{e}}_1^{\sigma}$ coincide at the structures of C_{2v} symmetry, but they can differ when the plane of symmetry is lost.

QTAIM –the β angle; the response to the torsion angle α

The response of the electronic structure to the twisting of the methylene group about the C_1-C_6 bond-path BCP is determined by the angle β, see Figure 1(a) for the definition, where we use β for QTAIM. Where β is the angle formed by the projections of the QTAIM $\underline{\mathbf{e}}_2$ eigenvectors on the X-Y plane with the Y axis, see Figure 1(a). More specifically, $\beta = \cos^{-1}(\underline{\mathbf{e}}_2 \cdot \underline{\mathbf{y}})$, see Table 6. Initially, at planar geometries (α=0°), β = 90° for the three states. To understand the behaviour of β during the bond twist it is convenient to think of the twist as the simultaneous rotation of the CH_2 group and the ring, in opposite directions. For a 'bona fide' π bond, as the two moieties rotate, the maximal π density at the BCP should have an intermediate orientation between the two normal vectors to the planes of the CH_2 group and the ring, and β should be approximately equal to 90°+α/2. This is approximately the case for the three states at **CI-63**, where the sum 90°+α/2 = 122° and the values of β are 125.29° for S_0, 130.26° for S_1 and 123.74° for S_2, see Table 6. Thus, the QTAIM $\underline{\mathbf{e}}_2$ eigenvector rotates about the C_1-C_6 bond-path as the methylene group is twisted, i.e. the direction of preferred electron accumulation changes.

The approximate relationship between α and β, β = 90°+α/2, does not hold at **CI-Perp**. The values of β at this structure are 0° for S_0 and S_1, and 90° for S_2, see Table 6. This is due to the fact that the double bond is broken at this geometry, see Figure 3(d-g), leaving a biradical in S_0 and S_1 and a zwitterion in S_2. In S_0 and

S_1, the ellipticities at the C_1-C_6 BCP are 0.025 and 0.012, respectively, see Table 1. The small values indicate that the charge density around the BCP is almost circular. This is consistent with the biradical character, with the two uncoupled electrons occupying the p orbitals on C_6 and C_1, which are orthogonal to each other, see Figure 3(g). The value of $\beta = 0°$ at **CI-Perp** indicates that the charge density on the C_6 p orbital is larger than that at C_1. This can be understood from MO theory, since the radical on C_6 is perfectly localized on that atom, while the one on C_1 is actually delocalized over the ring. In turn, the value of β at **CI-Perp** for S_2 is 90° and can be explained with the zwitterionic structure shown in Figure 3(f). The charge density on C_1 becomes larger than on C_6 because the p orbital on that atom is empty, and the larger charge density along the X direction results in a value of $\beta = 90°$.

To summarize, the changes in the charge density can be followed using the $\underline{\mathbf{e}}_1$-$\underline{\mathbf{e}}_2$-$\underline{\mathbf{e}}_3$ framework and the response of the QTAIM β angle. Initially, the $\underline{\mathbf{e}}_2$ eigenvector follows the twist for all the three states, as seen by the values of β at **CI-63**. However, in the final part of the twist the behavior of $\mathbf{e}_2$ is different for the biradical and zwitterionic states, as seen by the direction of $\underline{\mathbf{e}}_2$ at **CI-Perp**. For S_0 and S_1, the twisted structure is a biradical, and β has a value of 0°. In contrast, S_2 is a zwitterion with a β value of 90°. Thus, the changes in β can be used to distinguish between the biradical and zwitterionic character.

Stress tensor- the β_σ angle and the stiffness S_σ; the response to the torsion angle α

Now we will examine the value of β_σ derived from the stress tensor to gain more physical insights into the changes in the electronic structure. Previously, [30] the $\underline{\mathbf{e}}_2^{\sigma}$ eigenvector of the stress tensor has been found to provide insight into favorable electronic rearrangements. Here we follow bond path framework in the stress tensor formalism by calculating the angle β_σ formed by the $\underline{\mathbf{e}}_1^{\sigma}$ eigenvector and the plane of the ring. This angle is analogous to the angle β measured for the $\underline{\mathbf{e}}_2$ QTAIM eigenvector.

The values of β_σ give further information about the 'resistance to rotation' of the C_1-C_6 BCP bond-path and can be compared with the bond-path stiffness values S_σ in Table 4 and the QTAIM value β in Table 6. At planar geometries, β_σ is 90°. Similar to what has been discussed for β above, the values of β_σ at **CI-63** should be equal to $90°+\alpha/2$. This is the case for S_0 and S_2, where β_σ is 126.1° and 123.9°, respectively.

However, the value of β_σ for S_1 is 156.7° and corresponds, approximately, to the value of 90°+α. This can be understood considering the biradical character of S_1, see Figure 3(b) and Figure 3(e) where the results show that in S_1 the $\underline{\mathbf{e}}_1^{\sigma}$ eigenvector follows, approximately, the rotation of the π orbital on C_6. Thus, according to the stress tensor picture, the double bond is already broken at **CI-63** in the S_1 state. The differences between the values of β_σ for the S_0 and S_2 states, on one hand, and the S_1 state on the other are consistent with the lower ellipticity of S_1, see Table 1 and the lower stiffness S_σ of that state at **CI-63**, see Table 4. At **CI-Perp**, the values of β_σ coincide with those of β and can be understood with the biradical character of S_0 and S_1 and the zwitterionic character of S_2. S_2 also appears as the stiffest state with respect to rotation at **CI-Perp**, since the values of S_σ are 2.633 for S_0 and S_1 and 2.860 for S_2.

Stress tensor - Stiffness S_σ and atomic basin path sets

A direct interpretation of the stress tensor concept of BCP stiffness S_σ is apparent by the examination of the views of the basin path sets down the z-axis, see Figure 5(a-c) for the S_0(A), S_1(B) and S_2(A) **CI-63** states respectively and also see Table 4. The order of decreasing stiffness values S_σ, $S_0(A) > S_2(A) > S_1(B)$, matches the spread of the basin path sets. The greater the stiffness S_σ, the more the basin path sets spread out and the higher the ellipticity values ε and ε_σ.

The nature of the bond-path torsion unconstrained by symmetry can be seen in more detail by the consideration of both of the interatomic surface paths and the associated basin path sets in the form of the $\underline{\mathbf{e}}_1$-$\underline{\mathbf{e}}_2$ framework. The different stiffness values S_σ of the three states at **CI-63** can be visually compared in Figure 5(a-c). The nature of the bond-path torsion can be seen more in detail investigating how the different regions of the charge density respond to the bond torsion for a same state. The interatomic surface paths and the associated basin path sets in the form of the $\underline{\mathbf{e}}_1$-$\underline{\mathbf{e}}_2$-$\underline{\mathbf{e}}_3$ framework for the S_0 state are presented in Figure 5(d) and 5(e). Figure 5(d) presents the calculated basin path set starting the trajectories in the plane formed by $\underline{\mathbf{e}}_2$ and the C_1-C_6 bond path and Figure 5(e) in the plane formed by the C_1-C_6 bond path and $\underline{\mathbf{e}}_1$. It can be seen that the continuous surface of the basin path set defined by the plane containing $\underline{\mathbf{e}}_1$ and the torsional C_1-C_6 bond-path has a much larger surface area than that formed from the $\underline{\mathbf{e}}_2$ eigenvector and the torsional C_1-

C_6 bond-path, see Figure 5(e) and 5(d) respectively. We relate this result to the different topological stabilities of the charge density along the $\underline{\mathbf{e}}_1$ and $\underline{\mathbf{e}}_2$ directions where $\underline{\mathbf{e}}_2$ is the direction of preferred electronic accumulation. The charge density has the most stable morphology along the $\underline{\mathbf{e}}_2$ direction and therefore is less resistant to the applied twist. This is reflected in the small surface area of the basin path sets; see Figure 5(d). Conversely, $\underline{\mathbf{e}}_1$ is the direction of least facile electronic accumulation, and this results in a larger surface area for the basin path sets, see Figure 5(e), i.e. higher resistance to the twist. Notice also that the direction of torsion for the basin path sets defined by the plane including the $\underline{\mathbf{e}}_2$ eigenvector and torsional bond-path rotates in the opposite sense to that of the $\underline{\mathbf{e}}_1$ eigenvector according to the orientation presented.

To summarize the last two sections, with the stress tensor stiffness S_σ we have numerical descriptors of the resistance of the bond to the twist, while the atomic basin path sets provide a graphical representation. The state with the highest stiffness on the C_1-C_6 bond is the ground state, in agreement with chemical intuition and the MO picture. The stiffness is reflected in a larger spread of the basin path sets.

4. Conclusions.

Our QTAIM and stress tensor analysis, supported by MO theory, provides new insights into the double bond isomerization of fulvene in the ground and singlet excited states. We have been able use this new approach to characterize the electronic character of each state. Alternative methods previously used to explore excited state densities include the use of the electron localization function, which has been used to study the aromaticity of states of different multiplicity for several fulvene derivatives [39], as well as examining the absorption spectra and excited state dipole moments of four differently substituted fulvenes [38]. The results of this work can be compared with the picture given by Bonacic-Koutecky and Michl [24] These authors predict that for hydrocarbon double bonds, where the two groups at each side of the bond have similar electronegativities, the ground state at twisted geometries (α = 90.0°) has biradical character, while the excited state is zwitterionic. Our results agree partially with this picture, as S_0 is biradical and S_2 zwitterionic at **CI-Perp**. The zwitterionic character of S_2 is a result of a charge shift from C_6 to C_1 induced by the twist.

It only becomes apparent at the fully twisted structure. The difference with the picture of Bonacic-Koutecky and Michl lies in the appearance of a second biradical state, S_1. This can be understood considering that the biradical state of fulvene is analogous to a doubly degenerate state because of the presence of the cyclopentadienyl moiety [4].

The stress tensor provides new tools to describe the behavior of the charge density during the torsion. This includes the newly introduced stiffness S_σ which follows the physically intuitive picture of displaying a resistance to rotation. The physically intuitive effect of resistance to motion is visually apparent when viewing the spread of the basin path sets down the torsional bond-path axis, where the trajectories were started in the plane of the five carbon ring and methyl group for the C_1 and C_6 nuclei respectively. Higher values of the stiffness S_σ matched with a greater spreading out of the basin path sets in this case. In addition, for both QTAIM and the stress tensor the ellipticity decreased as the values of the stiffness decreased which indicates that less elliptical bond-path BCPs are more readily twisted than those with higher values of ellipticity.

Bond-path torsion was also characterized within QTAIM by twisted C_1 and C_6 atomic basin path sets as well as the $\underline{\mathbf{e}}_1$-$\underline{\mathbf{e}}_2$.$\underline{\mathbf{e}}_3$ framework of the Hessian of the density being rotated such that it was no longer contiguous with either the five carbon ring or the methyl group of the fulvene molecular graph. The basin path sets of the C_1 and C_6 nuclei with initial trajectories defined by the plane that included the entire bond-path and the $\underline{\mathbf{e}}_2$ eigenvector indicated the preferred morphology of bond-path torsion. Conversely, the $\underline{\mathbf{e}}_1$ eigenvector indicated the least preferred morphology of bond-path torsion. The surface area of the $\underline{\mathbf{e}}_1$ eigenvector defined C_1 and C_6 basin path sets was much greater than that of the $\underline{\mathbf{e}}_2$ eigenvector indicating the greater topological instability of the $\underline{\mathbf{e}}_1$ eigenvector defined bond-path torsion.

It is usually assumed that the bond always rotates in concert with the rotating nuclei. By monitoring the rotation of the bond following the $\underline{\mathbf{e}}_1$-$\underline{\mathbf{e}}_2$.$\underline{\mathbf{e}}_3$ framework of the Hessian of the density and the $\underline{\mathbf{e}}_1^{\sigma}$-$\underline{\mathbf{e}}_2^{\sigma}$-$\underline{\mathbf{e}}_3^{\sigma}$ framework of the stress tensor, we show that this assumption is not always correct. It depends on the nature of the state involved. We follow the rotation of the $\underline{\mathbf{e}}_1$-$\underline{\mathbf{e}}_2$.$\underline{\mathbf{e}}_3$ framework by monitoring the angles β and β_σ, which describe the torsion of the $\underline{\mathbf{e}}_2$ and $\underline{\mathbf{e}}_1^{\sigma}$ eigenvectors, for QTAIM and the stress tensor respectively.

Initially during the rotation, the C_1-C_6 bond retains its double bond character for the S_0 and S_2 states, and the angles β and β_σ rotate, approximately, in concert with the nuclei. In the final part of the rotation, for the S_0 state, the C_1-C_6 bond becomes a biradical and the $\underline{\mathbf{e}}_2$ and $\underline{\mathbf{e}}_1^{\sigma}$ eigenvectors get aligned with the p orbital on C_6. In contrast, the S_2 state becomes a zwitterion during the final part of the rotation, and the $\underline{\mathbf{e}}_2$ and $\underline{\mathbf{e}}_1^{\sigma}$ eigenvectors rotate backward to their initial position, in line with the p orbital on C_1. In turn, the rotation is different for the S_1 state. This state behaves as a biradical already during the beginning of the rotation, and the $\underline{\mathbf{e}}_1^{\sigma}$ eigenvector is aligned with the p orbital on C_6 already at half twisted geometries (**CI-63**). The biradical character of the S_1 state is also evident from the lower ellipticities and stiffness values.

To summarize, the stress tensor derived angle β_σ shows the response to the applied rotation α of the nuclei of the methylene group on the bond-path torsion, the value of β_σ is consistent with the stiffness S_σ and ellipticity ε_σ values. The stress tensor based descriptors also give a more consistent description of the bond torsion than the QTAIM ones. Thus, the differences between the states in the QTAIM derived β angle, in the absence of symmetry, are not as pronounced as those found for the stress tensor β_σ angle. Similarly, the proposed QTAIM stiffness $S = \lambda_3/|\lambda_2|$ does not describe properly the changes in bonding upon stretch of the C_1-C_6 bond. The QTAIM derived angle β, in the absence of symmetry, shows the preferred morphology of the bond-path BCP torsion, in terms of the basin paths sets of the C_1 and C_6 nuclei, these results are consistent with the stiffness S and ellipticity ε values.

Our work shows that the QTAIM and stress tensor analysis can be applied successfully to study processes in the excited state. This aspect seems especially promising. At present, the methods of electron density analysis have been applied almost exclusively to ground state properties and reactions. In addition, most methods for the analysis of the excited state are based on MO theory. In this context, QTAIM and the stress tensor can be valuable tools for the analysis of excited states, where changes in the charge density caused by the excitation often lead to unusual reactivity. Charge density changes are sufficient in the vicinity of conical intersection so that they can be clearly resolved from charge density derivatives, while the charge density itself may not have changed much. We will follow these ideas in future work using QTAIM.

Acknowledgements

The One Hundred Talents Foundation of Hunan Province and the aid program for Science and Technology Innovative Research Team in Higher Educational Institutions of Hunan Province are gratefully acknowledged for the support of S.J. and S.R.K. The National Natural Science Foundation of China is also gratefully acknowledged for the support of S.J. and S.R.K, project approval number: 21273069. L.B. acknowledges support from the Spanish Ministerio de Economía y Sostenibilidad (MINECO) (CTQ2011-26573 and UNGI08-4E-003 from FEDER (European Fund for Regional Development)), and the Catalan Agència de Gestió d'Ajuts Universitaris i de Recerca (SGR0528) and Direcció General de la Recerca (Xarxa de Referència en Química Teòrica i Computacional de Catalunya). The authors would also like to thank the referees for their considered and helpful comments.

References

[1] D. Polli, P. Altoè, O. Weingart, K. M. Spillane, C. Manzoni, D. Brida, G. Tomasello, G. Orlandi, P. Kukura, et al., "Conical intersection dynamics of the primary photoisomerization event in vision," *Nature* **467**(7314), 440–443 (2010) [doi:10.1038/nature09346].

[2] J. McMurry, *Organic Chemistry*, 8th ed., CengageBrain. com, UK (2010).

[3] G. G. Kochendoerfer and R. A. Mathies, "Spontaneous Emission Study of the Femtosecond Isomerization Dynamics of Rhodopsin," *J. Phys. Chem.* **100**(34), 14526–14532 (1996) [doi:10.1021/jp960509+].

[4] M. J. Bearpark, F. Bernardi, M. Olivucci, M. A. Robb, and B. R. Smith, "Can Fulvene S1 Decay Be Controlled? A CASSCF Study with MMVB Dynamics," *J. Am. Chem. Soc.* **118**(22), 5254–5260 (1996) [doi:10.1021/ja9542799].

[5] S. Ruiz-Barragan and L. Blancafort, "Photophysics of fulvene under the non-resonant stark effect. Shaping the conical intersection seam," *Faraday Discuss.* **163**(0), 497–512 (2013) [doi:10.1039/C3FD20155D].

[6] L. Blancafort, F. Gatti, and H.-D. Meyer, "Quantum dynamics study of fulvene double bond photoisomerization: The role of intramolecular vibrational energy redistribution and excitation energy," *J. Chem. Phys.* **135**(13), 134303 (2011) [doi:10.1063/1.3643767].

[7] D. Mendive-Tapia, B. Lasorne, G. A. Worth, M. A. Robb, and M. J. Bearpark, "Towards converging non-adiabatic direct dynamics calculations using frozen-width variational Gaussian product basis functions," *J. Chem. Phys.* **137**(22), 22A548 (2012) [doi:10.1063/1.4765087].

[8] D. Mendive-Tapia, B. Lasorne, G. A. Worth, M. J. Bearpark, and M. A. Robb, "Controlling the mechanism of fulvene S1/S0 decay: switching off the stepwise population transfer," *Phys. Chem. Chem. Phys.* **12**(48), 15725–15733 (2010) [doi:10.1039/C0CP01757D].

[9] A. F. Izmaylov, D. Mendive–Tapia, M. J. Bearpark, M. A. Robb, J. C. Tully, and M. J. Frisch, "Nonequilibrium Fermi golden rule for electronic transitions through conical intersections," *J. Chem. Phys.* **135**(23), 234106 (2011) [doi:10.1063/1.3667203].
[10] M. J. Bearpark, L. Blancafort, and M. J. Paterson, "Mapping the intersection space of the ground and first excited states of fulvene," *Mol. Phys.* **104**(5-7), 1033–1038 (2006) [doi:10.1080/00268970500418265].
[11] S. Belz, T. Grohmann, and M. Leibscher, "Quantum dynamical simulations for nuclear spin selective laser control of ortho- and para-fulvene," *J. Chem. Phys.* **131**(3), 034305 (2009) [doi:10.1063/1.3175800].
[12] R. F. W. Bader, *Atoms in Molecules: A Quantum Theory*, Oxford University Press, USA (1994).
[13] R. F. W. Bader, "Everyman's Derivation of the Theory of Atoms in Molecules," *J. Phys. Chem. A* **111**(32), 7966–7972 (2007) [doi:10.1021/jp073213k].
[14] C. F. Matta and R. F. W. Bader, "An Experimentalist's Reply to 'What Is an Atom in a Molecule?,'" *J. Phys. Chem. A* **110**(19), 6365–6371 (2006) [doi:10.1021/jp060761+].
[15] P. L. A. Popelier, *Atoms in Molecules: An Introduction*, Pearson Education, Harlow (1999).
[16] A. Tachibana, "Electronic energy density in chemical reaction systems," *J. Chem. Phys.* **115**(8), 3497–3518 (2001) [doi:doi:10.1063/1.1384012].
[17] P. Szarek and A. Tachibana, "The field theoretical study of chemical interaction in terms of the Rigged QED: new reactivity indices," *J. Mol. Model.* **13**(6-7), 651–663 (2007) [doi:10.1007/s00894-007-0215-6].
[18] A. Holas and N. H. March, "Exact exchange-correlation potential and approximate exchange potential in terms of density matrices," *Phys. Rev. A* **51**(3), 2040–2048 (1995) [doi:10.1103/PhysRevA.51.2040].
[19] L. J. Bartolotti and R. G. Parr, "The concept of pressure in density functional theory," *J. Chem. Phys.* **72**(3), 1593–1596 (1980) [doi:doi:10.1063/1.439358].
[20] R. F. W. Bader, T. T. Nguyen-Dang, and Y. Tal, "Quantum topology of molecular charge distributions. II. Molecular structure and its change," *J. Chem. Phys.* **70**(9), 4316–4329 (1979) [doi:doi:10.1063/1.438006].
[21] A. Tachibana, "Spindle structure of the stress tensor of chemical bond," *Int. J. Quantum Chem.* **100**(6), 981–993 (2004) [doi:10.1002/qua.20258].
[22] A. Guevara-García, P. W. Ayers, S. Jenkins, S. R. Kirk, E. Echegaray, and A. Toro-Labbe, "Electronic Stress as a Guiding Force for Chemical Bonding," pp. 1–22, Springer Berlin Heidelberg (2011).
[23] L. Blancafort, P. Celani, M. J. Bearpark, and M. A. Robb, "A valence-bond-based complete-active-space self-consistent-field method for the evaluation of bonding in organic molecules," *Theor. Chem. Acc.* **110**(2), 92–99 (2003) [doi:10.1007/s00214-003-0459-x].
[24] V. Bonačić-Koutecký, J. Koutecký, and J. Michl, "Neutral and Charged Biradicals, Zwitterions, Funnels in S1, and Proton Translocation: Their Role in Photochemistry, Photophysics, and Vision," *Angew. Chem. Int. Ed. Engl.* **26**(3), 170–189 (1987) [doi:10.1002/anie.198701701].
[25] R. F. W. Bader, "Bond Paths Are Not Chemical Bonds," *J. Phys. Chem. A* **113**(38), 10391–10396 (2009) [doi:10.1021/jp906341r].
[26] R. G. A. Bone and R. F. W. Bader, "Identifying and Analyzing Intermolecular Bonding Interactions in van der Waals Molecules†," *J. Phys. Chem.* **100**(26), 10892–10911 (1996) [doi:10.1021/jp953512m].
[27] S. Jenkins and M. I. Heggie, "Quantitative analysis of bonding in 90° partial dislocation in diamond," *J. Phys. Condens. Matter* **12**(49), 10325–10333 (2000) [doi:10.1088/0953-8984/12/49/3].
[28] S. Jenkins, "Direct space representation of metallicity and structural stability in SiO solids," *J. Phys. Condens. Matter* **14**(43), 10251–10263 (2002) [doi:10.1088/0953-8984/14/43/321].
[29] R. F. W. Bader and H. Essén, "The characterization of atomic interactions," *J. Chem. Phys.* **80**(5), 1943–1960 (1984) [doi:doi:10.1063/1.446956].
[30] P. W. Ayers and S. Jenkins, "An electron-preceding perspective on the deformation of materials," *J. Chem. Phys.* **130**(15), 154104–154104–11 (2009) [doi:10.1063/1.3098140].
[31] S. Jenkins, S. R. Kirk, A. S. Cote, D. K. Ross, and I. Morrison, "Dependence of the normal modes on the electronic structure of various phases of ice as calculated by ab initio methods," *Can. J. Phys.* **81**, 225–231(7) (2003).

[32] R. F. W. Bader, "Quantum topology of molecular charge distributions. III. The mechanics of an atom in a molecule," *J. Chem. Phys.* **73**(6), 2871–2883 (1980) [doi:doi:10.1063/1.440457].
[33] P. Szarek, Y. Sueda, and A. Tachibana, "Electronic stress tensor description of chemical bonds using nonclassical bond order concept," *J. Chem. Phys.* **129**(9), 094102–094102–16 (2008) [doi:doi:10.1063/1.2973634].
[34] F. Sicilia, M. J. Bearpark, L. Blancafort, and M. A. Robb, "An analytical second-order description of the S 0 /S 1 intersection seam: fulvene revisited," *Theor. Chem. Acc.* **118**(1), 241–251 (2007) [doi:10.1007/s00214-007-0320-8].
[35] M. Frisch, G. Trucks, H. Schlegel, G. Scuseria, M. Robb, J. Cheeseman, J. Montgomery, T. Vreven, K. Kudin, et al., *Gaussian 03, Revision E.01*, Gaussian, Inc., Wallingford, CT (2003).
[36] T. A. Keith, *AIMAll*, TK Gristmill Software, Overland Park KS, USA (2012).
[37] J. E. Kent, P. J. Harman, and M. F. O'Dwyer, "Photochemistry of benzene isomers. 1. Fulvene and 3,4-dimethylenecyclobutene," *J. Phys. Chem.* **85**(19), 2726–2730 (1981) [doi:10.1021/j150619a007].
[38] M. Rosenberg, H. Ottosson, and K. Kilså, "Influence of excited state aromaticity in the lowest excited singlet states of fulvene derivatives," *Phys. Chem. Chem. Phys.* **13**(28), 12912–12919 (2011) [doi:10.1039/C0CP02821E].
[39] C. Dahlstrand, M. Rosenberg, K. Kilså, and H. Ottosson, "Exploration of the π-Electronic Structure of Singlet, Triplet, and Quintet States of Fulvenes and Fulvalenes Using the Electron Localization Function," *J. Phys. Chem. A* **116**(20), 5008–5017 (2012) [doi:10.1021/jp3032397].

Figure 1. A schematic shows an aerial view down the C_1-C_6 bond-path axis, of the fulvene molecule and the orientation of the Cartesian coordinate system used throughout this study, see sub-figures (a). To illustrate the definition of α; the angle of mechanical twist of the methylene group and β and β_σ the QTAIM and stress tensor responses respectively of the C_1-C_6 BCP $\underline{\mathbf{e}}_2$ for QTAIM and C_1-C_6 BCP $\underline{\mathbf{e}}_1^{\sigma}$ for the stress tensor. The geometries, molecular graphs and numbering schemes of the nuclei used in this study are shown in sub-figures (b)-(d), see also the main text for further explanation and also Table 1 and Table 2.

Figure 2. Potential energy profile along the planar decay coordinate Q_1 (energies in eV). In sub-figure (b) Potential energy surface along Q_1 and Q_2 showing the conical intersection seam.

Figure 3. Fulvene resonance structures. In sub-figures (a)-(c) the S_0 - S_2 states at **S_0-Min** are shown; in sub-figures the (d)-(f) S_0 - S_2 states at **CI-Perp**; in sub-figure (g) C_1 and C_6 p orbitals at the **CI-Perp** geometry.

Figure 4. The stress tensor ellipticity ε_σ against the QTAIM ellipticity ε for the C-C BCPs is shown in sub-figure (a), see also Table 1 for the electronic states at the planar molecular graphs **S_0-Min**, **S_1-Min** and **CI-Plan** (α = 0.0°). The linear fit for the values of the C_1-C_6 BCP is shown separately as a dashed line, with gradient 0.461. The solid line is fitted to the remaining C-C BCPs, the gradient and correlation coefficient are 0.460 and 0.996 respectively. The stress tensor ellipticity ε_σ against the QTAIM ellipticity ε for the C-C BCPs is shown in sub-figure (b), see also Table 1 for the electronic states at structure **CI-63**. The linear fit for the values of the C_1-C_6 BCP is shown separately as a dashed line, with gradient and correlation coefficient 0.581. The solid line is fitted to the remaining C-C BCPs, the gradient and correlation coefficient are 0.470 and 0.999 respectively. The stress tensor ellipticity ε_σ against the QTAIM ellipticity ε for the C-C BCPs is shown in sub-figure (c), see also Table 1 for the electronic states at structure **CI-Perp** (α = 90.0°). The linear fit for the values of the C_1-C_6 BCP is shown separately as a dashed line, with gradient 0.665. The solid line is fitted to the remaining C-C BCPs, the gradient and correlation coefficient are 0.499 and 0.998 respectively.

Figure 5. Views of the gradient vector field distribution $\nabla\rho(\mathbf{r})$ down the Z-axis of the atomic basin paths sets of the C_6 and C_1 nuclei are presented in sub-figures (a)-(f) where the $\underline{\mathbf{e}}_1$ and $\underline{\mathbf{e}}_2$ interatomic surface eigenvector paths defined at the C_1-C_6 BCP, are highlighted in red. The atomic basin paths sets of the C_6 and C_1 nuclei are defined by the planes of

the CH_2 and five membered ring for the three **CI-63** states, $S_0(A)$, $S_1(B)$ and $S_2(A)$ and for **CI-Perp** $S_2(A_1)$ state, see sub-figures (a)-(c) and (d) respectively. The atomic basin paths set of the C_6 and C_1 nuclei for the **CI-63** state, $S_0(A)$ is defined by the plane that includes the $\underline{\mathbf{e}}_2$ inter-atomic surface path that passes along the length of the C1-C6 torsional bond-path, see sub-figure (e) the equivalent plane for the $\underline{\mathbf{e}}_1$ inter-atomic surface is presented in (f).

Table 1. The QTAIM and stress tensor ellipticities, ε and ε_σ respectively for each of the unique BCPs with the associated bond-paths for the different molecular graphs of the ground S_0 and exited electronic states, S_1 and S_2. The numbering scheme of the nuclei and the geometries of the electronic states of the fulvene molecule are given in Figure 1. The stress tensor ellipticity $\varepsilon_\sigma = (\lambda_1{}^\sigma/\lambda_2{}^\sigma)$ -1 which is the same form as that of QTAIM.

ellipticity	**S_0-Min**, α = 0.0°			**S_1-Min**, α = 0.0°			**CI-Plan**, α = 0.0°			**CI-63**[a], α = 63.0°			**CI-Perp**, α = 90.0°		
Bond-path	$S_0(A_1)$	$S_1(B_2)$	$S_2(A_1)$	$S_0(A_1)$	$S_1(B_2)$	$S_2(A_1)$	$S_0(A_1)$	$S_1(B_2)$	$S_2(A_1)$	$S_0(A)$	$S_1(B)$	$S_2(A)$	$S_0(A_2)$	$S_1(B_1)$	$S_2(A_1)$
ε (QTAIM)															
C_1-C_2 = C_1-C_4	0.098	0.269	0.171	0.138	0.257	0.189	0.150	0.261	0.237	0.169	0.255	0.213	0.190	0.254	0.338
C_1-C_6	0.344	0.130	0.274	0.252	0.095	0.237	0.229	0.089	0.123	**0.150**	**0.047**	**0.112**	0.025	0.012	0.157
C_2-C_3 = C_4-C_5	0.365	0.138	0.088	0.293	0.129	0.103	0.268	0.123	0.288	0.290	0.128	0.140	0.293	0.131	0.306
C_3-C_5	0.102	0.301	0.245	0.158	0.335	0.218	0.183	0.353	0.303	0.138	0.332	0.190	0.117	0.319	0.264
ε_σ (Stress Tensor)															
C_1-C_6	0.118	0.033	0.094	0.093	0.009	0.086	0.085	0.007	0.027	0.068	0.008	0.044	0.015	0.006	0.103

Table 2. P_{ij} bond indices and localized orbital occupations for the S_0, S_1 and S_2 states at the different structures. See Figure 1 for the atom numbering scheme.

P_{ij} indices	**S_0-Min**			**S_1-Min**			**CI-Plan**			**CI-63**			**CI-Perp**		
	$S_0(A_1)$	$S_1(B_2)$	$S_2(A_1)$	$S_0(A_1)$	$S_1(B_2)$	$S_2(A_1)$	$S_0(A_1)$	$S_1(B_2)$	$S_2(A_1)$	$S_0(A)$	$S_1(B)$	$S_2(A)$	S_0 (A_2)	$S_1(B_1)$	$S_2(A_1)$
C_1-C_2 = C_1-C_4	0.072	0.291	0.156	0.108	0.345	0.190	0.116	0.358	0.203	0.160	0.365	0.195	0.204	0.367	0.212
C_1-C_6	0.592	-0.048	0.406	0.549	-0.109	0.331	0.536	-0.123	0.311	0.549	-0.147	0.186	0.556	-0.159	0.000
C_2-C_3 = C_4-C_5	0.592	0.097	-0.123	0.509	0.060	-0.091	0.464	0.054	-0.075	0.493	0.063	0.010	0.487	0.076	0.333
C_3-C_5	0.068	0.453	0.274	0.163	0.550	0.226	0.216	0.577	0.2198	0.099	0.555	0.150	0.032	0.541	0.290
Localized orbital occupations															
C_1	0.963	1.145	1.036	0.947	1.066	1.030	0.931	1.045	1.031	0.912	1.069	1.035	0.899	1.083	1.409
$C_2 = C_4$	1.027	0.878	0.979	1.058	0.938	0.982	1.074	0.954	0.984	1.077	0.938	1.013	1.078	0.931	1.174
$C_3 = C_5$	0.998	1.028	0.994	0.994	1.027	0.976	0.988	1.023	0.968	0.980	1.026	0.985	0.972	1.029	1.121
C_6	0.988	1.043	1.018	0.948	1.005	1.055	0.944	1.000	1.075	0.973	1.002	0.970	1.000	1.000	0.000

Table 3. The QTAIM bond-path lengths (BPL) in Ångstrom for the molecular graphs of the ground S_0 and exited electronic states, S_1 and S_2, see also Table1 and Figure 1. The BPLs are state independent and so only one BPL value is given for each state. The bond-paths are nearly linear in all cases, and their lengths are approximately equal to the interatomic distances (bond lengths).

BPL	**S_0-Min**	**S_1-Min**	**CI-Plan**	**CI-63**	**CI-Perp**
Bond-path	$S_0(A_1)$, $S_1(B_2)$, $S_2(A_1)$	$S_0(A_1)$, $S_1(B_2)$, $S_2(A_1)$	$S_0(A_1)$, $S_1(B_2)$, $S_2(A_1)$	$S_0(A)$, $S_1(B)$, $S_2(A)$	$S_0(A_2)$, $S_1(B_1)$, $S_2(A_1)$
C_1-C_2 = C_1-C_4	1.480	1.400	1.373	1.410	1.425
C_1-C_6	1.349	1.498	1.578	1.482	1.478
C_2-C_3 = C_4-C_5	1.356	1.472	1.531	1.462	1.425
C_3-C_5	1.484	1.361	1.320	1.371	1.414

Table 4. The QTAIM 'stiffness' values, $S = [\lambda_3/|\lambda_2|]$ and stress tensor 'stiffness' values, $S_\sigma = [|\lambda_1{}^\sigma|/\lambda_3{}^\sigma]_\sigma$ respectively, evaluated at the C_1-C_6 BCPs.

Stiffness	**S_0-Min**			**S_1-Min**			**CI-Plan**			**CI-63**			**CI-Perp**		
	$S_0(A_1)$	$S_1(B_2)$	$S_2(A_1)$	$S_0(A_1)$	$S_1(B_2)$	$S_2(A_1)$	$S_0(A_1)$	$S_1(B_2)$	$S_2(A_1)$	$S_0(A)$	$S_1(B)$	$S_2(A)$	$S_0(A_2)$	$S_1(B_1)$	$S_2(A_1)$
S	0.601	0.485	0.561	0.774	0.677	0.766	0.821	0.728	0.752	0.692	0.647	0.680	0.632	0.632	0.663
S_σ	3.974	3.829	3.943	2.720	2.511	2.687	2.525	2.343	2.375	2.706	2.597	2.667	2.633	2.633	2.860

Table 5. The QTAIM net charge q(A) of atoms C_1, C_6, H_{11} and H_{12}. See Table 1 and the caption of Table 2 for more details.

q(A)	**S_0-Min**			**S_1-Min**			**CI-Plan**			**CI-63**			**CI-Perp**		
Atom A	$S_0(A_1)$	$S_1(B_2)$	$S_2(A_1)$	$S_0(A_1)$	$S_1(B_2)$	$S_2(A_1)$	$S_0(A_1)$	$S_1(B_2)$	$S_2(A_1)$	$S_0(A)$	$S_1(B)$	$S_2(A)$	$S_0(A_2)$	$S_1(B_1)$	$S_2(A_1)$
C_1	0.009	0.003	0.008	0.085	-0.053	0.008	0.078	-0.056	-0.025	0.101	-0.067	-0.013	0.110	-0.086	-0.397
C_6	0.093	0.071	0.090	0.080	0.024	-0.005	0.063	0.006	0.684	0.059	0.040	0.064	0.046	0.056	0.812
$H_{11} = H_{12}$	-0.043	-0.053	-0.050	-0.022	-0.020	-0.027	-0.009	-0.007	-0.024	0.018	-0.023	-0.023	-0.021	-0.029	-0.006

Table 6. The angle $\beta = \cos^{-1}(\underline{\mathbf{e}}_2 \cdot \underline{\mathbf{y}})$ for the $\underline{\mathbf{e}}_2$ eigenvectors of the C_1-C_6 BCP (torsional bond-path) from the QTAIM and angle $\beta_\sigma = \cos^{-1}(\underline{\mathbf{e}}_1^{\sigma} \cdot \underline{\mathbf{y}})$ for the stress tensor for fulvene for a range of molecular graphs and electronic states, see Table 1 and the associated caption. All values of β are confined to the X-Y plane. The angle α gives the mechanical twist imposed on the CH_2 unit, further explanation of the torsional bond-path C_1-C_6, the angles α and β and the coordinate system used is provided in Figure 1. See also Table 1.

β, β_σ	**S_0-Min**			**S_1-Min**			**CI-Plan**			**CI-63**			**CI-Perp**		
Bond-path C_1-C_6	$S_0(A_1)$	$S_1(B_2)$	$S_2(A_1)$	$S_0(A_1)$	$S_1(B_2)$	$S_2(A_1)$	$S_0(A_1)$	$S_1(B_2)$	$S_2(A_1)$	$S_0(A)$	$S_1(B)$	$S_2(A)$	$S_0(A_2)$	$S_1(B_1)$	$S_2(A_1)$
QTAIM $\beta = \cos^{-1}(\underline{\mathbf{e}}_2 \cdot \underline{\mathbf{y}})$	90.0	90.0	90.0	90.0	90.0	90.0	90.0	90.0	90.0	125.29	130.26	123.74	0.0	0.0	90.0
Stress tensor $\beta_\sigma = \cos^{-1}(\underline{\mathbf{e}}_1^{\sigma} \cdot \underline{\mathbf{y}})$	90.0	90.0	90.0	90.0	90.0	90.0	90.0	90.0	90.0	126.06	156.67	123.89	0.0	0.0	90.0